



# On the General Mechanism for the Gas-phase Reaction of Methanimine with a Radical Species in the Interstellar Medium: Some Failures and an Important Success

Hexu Ye , Silvia Alessandrini , and Cristina Puzzarini

Dipartimento di Chimica “Giacomo Ciamician,” Università di Bologna, Via F. Selmi, 2, Bologna, I-40126, Italy; [silvia.alessandrini7@unibo.it](mailto:silvia.alessandrini7@unibo.it), [cristina.puzzarini@unibo.it](mailto:cristina.puzzarini@unibo.it)

Received 2023 August 24; revised 2023 November 13; accepted 2023 December 2; published 2024 February 5

## Abstract

The gas-phase reactions of methanimine ( $\text{CH}_2\text{NH}$ ) with small radicals, such as CN, CP, CCH, and OH, have been extensively studied theoretically in the literature, and the presence of a common, general reaction mechanism has been postulated. Since methanimine is considered the main precursor of *complex imines* in the interstellar medium (ISM), the present study extends the investigation of its reaction with other small radicals that have already been detected in the ISM. These are SiN, SH, NO, NS, HCO, HCS, and  $\text{C}_3\text{N}$ . The corresponding products are easily formulated on the basis of the aforementioned general mechanism, and to understand whether they can be formed in the ISM, a preliminary thermochemical study has been carried out. The only exothermic addition reaction is that occurring between  $\text{CH}_2\text{NH}$  and the  $\text{C}_3\text{N}$  radical. This reaction has been further investigated in order to accurately characterize its reactive potential energy surface, which has then been employed in *ab initio* transition state theory calculations to derive global rate coefficients. The products of the  $\text{CH}_2\text{NH} + \text{C}_3\text{N}$  reaction are new potential interstellar species, namely, the *Z* and *E* isomers of  $\text{HNCHCCCN}$  and  $\text{CH}_2\text{NCCCN}$ . For the first time, their structural characterization has been reported. In addition, this work investigates the possibility of H-abstraction processes for each radical species considered, and re-examines the  $\text{CH}_2\text{NH} + \text{CP}$  reaction to derive the corresponding rate constants, that were still missing in the literature.


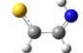


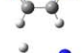
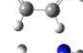
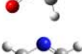
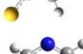
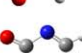
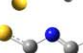
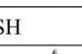


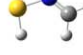
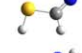


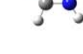




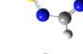
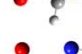

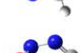
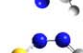
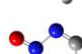
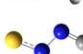


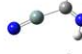


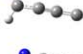

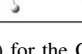
*Unified Astronomy Thesaurus concepts:* [Astrochemistry \(75\)](#); [Reaction rates \(2081\)](#); [Molecular reactions \(2226\)](#); [Neutral-neutral reactions \(2265\)](#)

## 1. Introduction

In the last years, powerful radioastronomical facilities such as the Atacama Large Millimeter/submillimeter Array (Wootten & Thompson 2009), Green Bank Telescope (Prestage et al. 2009), and YEBES (Tercero et al. 2021) have allowed extremely high-sensitivity and high-resolution ( $0.02 \text{ km s}^{-1}$ ) spectral line surveys such as GOTHAM (McGuire et al. 2020) and QUIJOTE (Cernicharo et al. 2022a). Owing to the support of laboratory spectroscopy investigations, these have led to the discovery of tens of new molecules in space (see, e.g., Lee et al. 2021; Cernicharo et al. 2022b; Fuentetaja et al. 2022; Sita et al. 2022). However, while the census of the interstellar species has been updating nearly on a biweekly basis, the progress in the derivation of efficient formation routes for the newly detected molecular systems as well as for many of those identified in the past is not able to keep up pace. As a consequence, we are not able to explain the presence of all the detected molecules and their abundance, as well as to indicate what new molecules should be searched for (Puzzarini 2020). It would thus be particularly useful to rationalize interstellar chemistry in terms of classes of reactions. These are collections of reactions in which one of the two reactants is the same while the other reactive species is varied, but the mechanism remains the same. A general mechanism to be effective must meet the constraints imposed by the physical conditions of the interstellar medium (ISM): because of the low temperatures, reactions must be exothermic and present only submerged barriers. However,

quantum effects such as H-atom tunneling and intersystem crossing could play a role in interstellar chemistry (Shannon et al. 2013; Ocaña et al. 2019; Recio et al. 2022).

In the present work, we focus on the general mechanism that involves methanimine ( $\text{CH}_2\text{NH}$ ) as the main reactant and a radical species, which is instead varied.  $\text{CH}_2\text{NH}$  is a widespread molecule that has been detected in several astronomical sources (Godfrey et al. 1973; Dickens et al. 1997; Turner et al. 1999; Dore et al. 2012), and it is considered the precursor of several complex imines (Puzzarini 2022), which are in turn considered important prebiotic species (Rivilla et al. 2019; Baiano et al. 2020; Shingledecker et al. 2020; Puzzarini 2022). In prior works, the reactions of  $\text{CH}_2\text{NH}$  with OH (Vazart et al. 2016), CN (Vazart et al. 2015; Barone & Puzzarini 2022), CCH (Lupi et al. 2020), and CP (Alessandrini et al. 2021) have been found to share the same pathways and thus, to lead to the identification of a general mechanism for the reaction between  $\text{CH}_2\text{NH}$  and a generic radical species X (Puzzarini 2022). Here, we aim at a systematic investigation of the gas-phase  $\text{CH}_2\text{NH} + \text{X}$  reaction, thereby considering different open-shell partners, with all of them being species already detected in the ISM. These are (i) SH (Neufeld et al. 2012) and SiN (Turner 1992), second-row analogs of the OH and CN radicals; (ii) the NO (Liszt & Turner 1978) and NS (Gottlieb et al. 1975) species; (iii) HCO, HCS (Snyder et al. 1976; Agúndez et al. 2018), and  $\text{C}_3\text{N}$  (Friberg et al. 1980), which represent a class of medium-sized radicals with three or more atoms. All these species have an unpaired electron, and thus, they have a doublet electronic ground state, similar to the other radicals for which the general mechanism holds. Furthermore, the reactions of  $\text{CH}_2\text{NH}$  with OH, CN and CCH are demonstrated to provide important formation routes for formamide and methanimidic acid (Vazart et al. 2016), cyanomethanimine (Barone & Puzzarini 2022),

		junChS	revDSD/ junTZ		junChS	revDSD/ junTZ	
	HCO	-113.8295 $E_h$	-113.6932 $E_h$	HCS	-436.6605 $E_h$	-436.4356 $E_h$	
PZc		71.53	70.88	PZc		47.32	47.47
PZt		68.50	67.12	PZt		43.99	43.06
PEc		86.44	85.33	PEc		60.71	60.52
PEt		63.36	61.96	PEt		38.61	37.52
PNc		62.02	59.72	PNc		51.10	47.82
PNt		68.86	66.43	PNt		66.16	64.41
	SH	-398.6083 $E_h$	-398.4400 $E_h$	SH	-398.6083 $E_h$	-398.4400 $E_h$	
PZc		80.75	81.62	PNc		136.95	138.47
PZt		79.86	80.88	PNt		135.30	136.44
PEc		78.44	79.41	PF		40.86	41.78
PEt		82.60	83.65				
	NO	-129.8797 $E_h$	-129.7342 $E_h$	NS	-452.7300 $E_h$	-452.4930 $E_h$	
PZc		238.87	240.92	PZc		163.77	159.27
PZt		246.48	249.68	PZt		173.97	169.81
PEc		244.39	246.62	PEc		171.76	167.29
PEt		258.64	261.06	PEt		175.19	170.61
PNc		268.19	268.54	PNc		220.95	212.20
PNt		266.13	265.99	PNt		235.96	230.33
	SiN	-343.9757 $E_h$	-343.7651 $E_h$	C <sub>3</sub> N	-168.8035 $E_h$	-168.5660 $E_h$	
PZ		196.10	178.43	PZ		-143.90	-166.74
PE		196.43	179.84	PE		-142.30	-165.04
PN		155.92	139.35	PN		-117.84	-142.31

**Figure 1.** ZPE-corrected junChS and revDSD/junTZ reaction energies (kilojoule per mole) for the  $\text{CH}_2\text{NH} + \text{X}$ , with  $\text{X} = \text{HCO}, \text{HCS}, \text{SH}, \text{NO}, \text{NS}, \text{SiN}, \text{C}_3\text{N}$ , addition reactions. The radical absolute energies (in Hartree,  $E_h$ ) are also reported. For  $\text{CH}_2\text{NH}$ , the absolute energy is  $-94.5815 E_h$  at the junChS level and  $-94.4509 E_h$  at the revDSD/junTZ level. The junChS and revDSD/junTZ electronic energies are augmented by harmonic ZPE corrections at the revDSD/junTZ level. For all reactions, the coproduct is always a H-atom, whose absolute energy is  $-0.5000 E_h$  at the junChS level and  $-0.4990 E_h$  at the revDSD/junTZ level.

and propargylimine (Lupi et al. 2020), respectively. Based on energetic considerations, the  $\text{CH}_2\text{NH} + \text{CP}$  reaction (Alessandrini et al. 2021) was suggested to form  $\text{HNCHCP}$  and  $\text{CH}_2\text{NCP}$ . However, kinetic considerations are necessary to confirm that these new substituted imines are good candidates for astronomical searches. For this reason, the present work reports kinetic calculations for all the  $\text{CH}_2\text{NH} + \text{X}$  processes (among those here considered) that were found energetically

open in the ISM conditions and also re-examines the  $\text{CH}_2\text{NH} + \text{CP}$  reaction, for which a kinetic analysis was still missing.

This paper is organized as follows. In the next section, the main details of the computational methodology employed in this work are provided (a more detailed account is reported in Appendix A). For each radical of the list above, the possible products of the reaction with methanimine have been derived

based on the general mechanism detailed in Puzzarini (2022), also considering H-abstraction processes. While endothermic reactions have been discarded after this first stage, for exothermic reactions, a complete and accurate characterization of the reactive potential energy surface (PES) has been carried out. This latter has then been employed to derive accurate kinetic constants for conditions relevant to the ISM. Finally, for new potential candidates for astronomical searches, a preliminary spectroscopic characterization has been performed. All results are presented and discussed in Section 3 and concluding remarks are drawn in the last section.

## 2. Computational Methodologies

To investigate the energetics of the  $\text{CH}_2\text{NH} + \text{X}$  reaction, with X being the HCO, HCS, NO, NS, SH, SiN, and  $\text{C}_3\text{N}$  radicals, the preliminary step is the geometry optimization of all reactants and potential products. For this purpose, the revDSDPBEP86 double-hybrid functional (Santra et al. 2019) in conjunction with the jun-cc-pVTZ basis set (Dunning 1989; Kendall et al. 1992; Woon & Dunning 1993; Dunning et al. 2001; Papajak & Truhlar 2011) has been employed in the unrestricted formalism (Sosa & Bernhard Schlegel 1986). These calculations always incorporate the D3BJ dispersion correction (Goerigk & Grimme 2011; Grimme et al. 2011). In the following, this level of theory is shortly denoted as revDSD/junTZ. As mentioned in the Introduction, the initial structure of each product has been deduced from the general mechanism proposed in Puzzarini (2022) and H-abstraction processes. The nature of each stationary point was verified by computing the corresponding Hessian at the same level of theory; this computation also provided the zero-point energy (ZPE) correction at the harmonic level.

On top of the revDSD/junTZ molecular structures, the quantum-chemical composite scheme denoted as “jun-Cheap” (junChS; Alessandrini et al. 2019) was employed to improve reactants and products electronic energies, and thus to accurately determine the exothermicity (or endothermicity) of the reaction under consideration. Details on the junChS approach can be found in Appendix A. As mentioned above, only exothermic processes have been retained for an extended investigation of the reaction mechanism. For them, the reactive PES has been mapped at the revDSD/junTZ level of theory. As usual, the transition states (TSs) found along the pathways have been connected to the corresponding minima (MIN) by means of the intrinsic reaction coordinate analysis (Fukui 1981). As above, Hessian calculations (at the revDSD/junTZ level) were employed to verify the nature of stationary points. Subsequently, the energy of the stationary points has been improved by exploiting the junChS approach and corrected for the harmonic revDSD/junTZ ZPE. To verify that static correlation is not relevant for the systems considered, the energetics for the reaction involving the  $\text{C}_3\text{N}$  radical have also been computed at the complete active space second-order perturbation theory (CASPT2; Roos et al. 1982; Andersson et al. 1990; Andersson et al. 1992; Celani & Werner 2000) in conjunction with the aug-cc-pVTZ basis set (Kendall et al. 1992; Woon & Dunning 1993), hereafter augTZ, with five active electrons in seven orbitals being used to generate the complete active space self-consistent field wave function.

For reactions open in interstellar conditions, the junChS energies were then employed to derive the rate constants in interstellar conditions. The Master Equation System Solver

(MESS) program (Georgievskii et al. 2013) has been used to obtain the global kinetic constants, thereby exploiting the ab initio transition state theory (AITSTME) and modeling the entrance channels using the phase-space theory (PST; Bao & Truhlar 2017). Rate coefficients have been simulated in different conditions: pressure has been varied from 1 to  $1 \times 10^{-12}$  atm and temperature in the 40–300 K range. These data have then been used to model the temperature dependence with the Arrhenius–Kooij expression (Kooij 1893), more details being provided in Appendix A. At this stage, the reaction between  $\text{CH}_2\text{NH}$  and CP was also reconsidered in order to derive accurate rate constants. For this purpose, its reactive PES has also been re-investigated at the revDSD/junTZ level of theory, with a particular focus on the entrance channels. As before, the junChS approach has been employed for obtaining improved energetics for the kinetic study.

Finally, products that are good candidates as interstellar species, have been spectroscopically characterized whenever no information was reported in the literature. Such a computational characterization is the first step toward their experimental laboratory investigation, the focus being on rotational spectroscopy. In particular, accurate rotational constants have been obtained by exploiting the so-called *Lego-brick* (template molecule pluslinear regression (TM +LR)) approach (Melli et al. 2021; Ye et al. 2022) for accurate equilibrium structures (and thus equilibrium rotational constants) and the B3LYP-D3BJ/jun-cc-pVDZ level of theory (hereafter B3LYP/junDZ; Becke 1988; Lee et al. 1988) for accounting for vibrational effects. A summary of the related computational details is reported in Appendix A.

## 3. Results and Discussion

In the following, the preliminary investigation of the thermochemistry associated with the reactions considered is discussed. Subsequently, the reactive PESs for the exothermic reactions are presented. This section is then concluded by reporting the results of the kinetic study.

### 3.1. Preliminary Thermochemical Investigation

The ZPE-corrected reaction energies of the  $\text{CH}_2\text{NH} + \text{X}$  processes, with X = HCO, HCS, SH, NO, NS, SiN,  $\text{C}_3\text{N}$ , are reported in Figure 1 for the products obtained from the general reaction mechanism (radical addition), while Figure 2 collects the thermodynamic data for the H-abstractions. Both figures compare the junChS and revDSD/junTZ results, and graphically show the structure of the products. Those in Figure 1 were obtained by considering the addition of the radical (X) to methanimine followed by a one- or two-step mechanism leading to hydrogen loss (see Figure 6 in Puzzarini 2022). In line with the general mechanism proposed in the literature, the products are in the form of Z- and E-HN=CH-X (denoted as PZ and PE, respectively), or in the form of  $\text{H}_2\text{C}=\text{N}-\text{X}$  (denoted as PN), where X is a generic radical. For HCO, HCS, NO, NS, and SH, different conformers are possible for a given E or Z isomer due to the different possible orientations of the added moiety. These conformers are indicated using the *cis/trans* nomenclature, and thus by appending a “c” or “t” to the PE, PZ, or PN acronyms. In addition, for the  $\text{CH}_2\text{NH} + \text{SH}$  reaction, the formation of thioformamide ( $\text{NH}_2\text{CHS}$ ) was also considered, in analogy to the mechanism observed for the  $\text{CH}_2\text{NH} + \text{OH}$  reaction, with formamide ( $\text{NH}_2\text{CHO}$ ) being

		junChS	revDSD/ junTZ			junChS	revDSD/ junTZ
HCO		-113.8295 $E_h$	-113.6932 $E_h$	HCS		-436.6605 $E_h$	-436.4356 $E_h$
PH1		1.06	7.02	PH1		-21.66	-13.99
PH2		50.67	53.17	PH2		27.95	32.16
PH3		32.34	33.95	PH3		9.62	12.93
SH		-398.6083 $E_h$	-398.4400 $E_h$	SH		-398.6083 $E_h$	-398.4400 $E_h$
PH1		-12.82	-4.74	PH3		16.62	22.18
PH2		34.95	41.41				
NO		-129.8797 $E_h$	-129.7342 $E_h$	NS		-452.7300 $E_h$	-452.4930 $E_h$
PH1		164.67	175.23	PH1		90.81	95.79
PH2		214.28	221.38	PH2		140.42	141.94
PH3		195.95	202.15	PH3		122.09	122.71
SiN		-343.9757 $E_h$	-343.7651 $E_h$	C <sub>3</sub> N		-168.8035 $E_h$	-168.5660 $E_h$
PH1		109.79	87.39	PH1		-220.59	-231.57
PH2		159.39	133.54	PH2		-170.99	-185.42
PH3		141.07	114.31	PH3		-189.31	-204.65

**Figure 2.** ZPE-corrected junChS and revDSD/junTZ reaction energies (kilojoule per mole) for the  $\text{CH}_2\text{NH} + \text{X}$ , with  $\text{X} = \text{HCO}, \text{HCS}, \text{SH}, \text{NO}, \text{NS}, \text{SiN}, \text{C}_3\text{N}$ , H-abstraction reactions. The radical absolute energies (in Hartree,  $E_h$ ) are also reported. For  $\text{CH}_2\text{NH}$ , the absolute energy is  $-94.5815 E_h$  at the junChS level and  $-94.4509 E_h$  at the revDSD/junTZ level. The junChS and revDSD/junTZ electronic energies are augmented by harmonic ZPE corrections at the revDSD/junTZ level. The absolute energies of  $\text{H}_2\text{CN}$ , *cis*-HCNH, and *trans*-HCNH are:  $-93.8126 E_h$ ,  $-93.7950 E_h$ , and  $-93.8024 E_h$ , respectively, at the revDSD/junTZ level, and  $-93.9418 E_h$ ,  $-93.9229 E_h$ , and  $-93.9299 E_h$ , respectively, at the junChS level.

formed via a TS located above the reactants (Vazart et al. 2016). In our case, in Figure 1, thioformamide and its coproduct (H-atom), indicated by the acronym PF, lie above the reactants by about  $40 \text{ kJ mol}^{-1}$ , thus being endothermic products that were not further investigated.

From the inspection of Figures 1 and 2, it is apparent that the revDSD and junChS energies agree—on average—within  $7 \text{ kJ mol}^{-1}$ , with the largest deviations (about  $20 \text{ kJ mol}^{-1}$ ) being noted for the reactions involving SiN and C<sub>3</sub>N. The junChS energies indicate that six reactions out of the seven considered, have addition products lying higher in energy than the reactants. These six processes are those involving the HCO, HCS, SH, NO, NS, and SiN radicals. Therefore, they cannot proceed in the gas phase in the conditions typical of the ISM following the general mechanism mentioned above. The only exothermic reaction that concerns the addition process is that involving C<sub>3</sub>N, which leads to *Z*-HN=CH-C<sub>3</sub>N+H (PZ), *E*-HN=CH-C<sub>3</sub>N+H (PE), and H<sub>2</sub>C=N-C<sub>3</sub>N+H (PN), these being located at  $143.9$ ,  $142.3$  and  $117.8 \text{ kJ mol}^{-1}$  below the reactants, respectively.

For what concerns H-abstraction processes, methanimine has three hydrogen atoms that can be extracted by the radical. Therefore, the products are labeled as PH1, PH2, and PH3. For HCO, NO, NS, and SiN, all three possible abstractions are

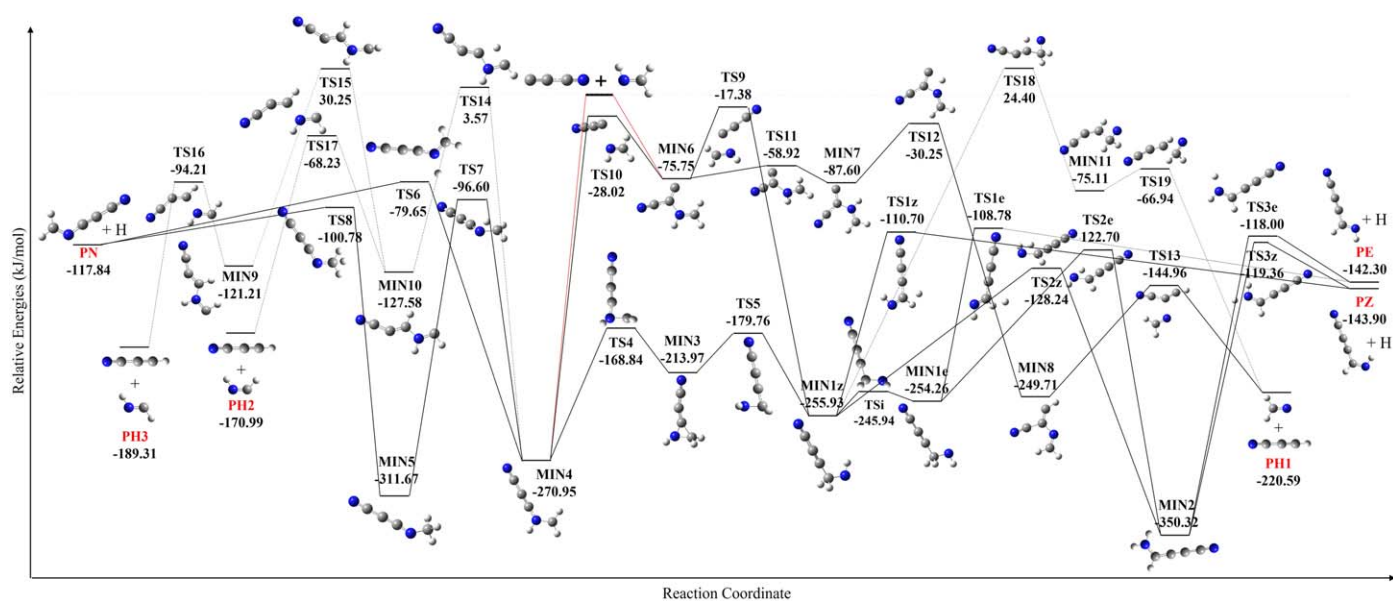
endothermic, as evident from Figure 2. Thus, these processes cannot occur in the ISM. One H-abstraction channel was found exothermic for both HCS and SH, while all three H-abstractions are exothermic in the case of the C<sub>3</sub>N radical. These processes, together with the only possible exothermic addition, are analyzed in detail in the next section.

### 3.2. Reactive Potential Energy Surfaces

According to the results presented above (Figures 1 and 2), the addition of the C<sub>3</sub>N radical on methanimine and the corresponding H-abstraction processes are promising interstellar processes. Therefore, the  $\text{CH}_2\text{NH} + \text{C}_3\text{N}$  reaction has been further investigated to derive the complete reactive PES. The other exothermic processes in Figure 2, i.e., the H-abstractions leading to H<sub>2</sub>S + H<sub>2</sub>CN and H<sub>2</sub>CS + H<sub>2</sub>CN, are discussed in Appendix B.

For  $\text{CH}_2\text{NH} + \text{C}_3\text{N}$ , the reaction mechanism is depicted in Figure 3, where the red lines represent the barrierless entrance channels toward MIN4 and MIN6. The former intermediate results from the addition of the first carbon atom of C<sub>3</sub>N to the N-end of CH<sub>2</sub>NH. MIN6 is also formed from the approach to the N-end of methanimine, but this involves the second carbon atom of C<sub>3</sub>N, and leads to the formation of a carbene-like structure. These minima interconvert via TS10





**Figure 3.** The  $C_3N + CH_2NH$  PES. The junChS relative energies, corrected for the harmonic revDSD/junTZ ZPE contribution, are reported.

( $-28.02 \text{ kJ mol}^{-1}$ ). From MIN6, the system can evolve toward PH1 (lying  $220.6 \text{ kJ mol}^{-1}$  below the reactants) in a three-step submerged pathway. The same product can be formed from MIN1z in two steps involving TS18 ( $+24 \text{ kJ mol}^{-1}$ ), MIN11 ( $-75.11 \text{ kJ mol}^{-1}$ ), and TS19 ( $-66.9 \text{ kJ mol}^{-1}$ ). This last path is similar to those leading to PH2 and PH3, which are instead obtained from MIN4. The latter evolves to MIN10 (at  $-127.6 \text{ kJ mol}^{-1}$ ), via TS14 located  $3.6 \text{ kJ mol}^{-1}$  above the reactants at the junChS level. MIN10 can then evolve to (i)  $HC_3N + cis\text{-HCNH}$  (PH2) in a one-step process that is submerged with respect to the reactants, and to (ii)  $HC_3N + trans\text{-HCNH}$  (PH3) via a two-step process that involves TS15 located above the reactants by  $30 \text{ kJ mol}^{-1}$ . While PH1 can be formed in the gas phase via a submerged pathway, the formation of PH2 can only occur if the TS14 barrier is overcome via hydrogen tunneling. For PH3, tunneling effects need to be invoked to pass both TS14 and TS15 barriers. Even if H-atom tunneling can play an important role in astrochemical reactions at low temperatures (Shannon et al. 2013; Ocaña et al. 2019), our calculations suggest that the formation of PH1 is the most probable H-abstraction mechanism.

The H-abstraction channel leading to PH1 competes with the formation of PZ, PE, and PN, which are the main products according to the general mechanism. From MIN6, the reaction can evolve toward MIN1z, which can interconvert through a low barrier to MIN1e. From MIN1z and MIN1e, PZ and PE are formed via one- or two-step paths according to the general mechanism. From MIN1z, the reaction can also proceed toward MIN3 (a cyclic intermediate), and from this, to MIN4. Thus, MIN6 and MIN4 are connected through two possible pathways, either involving one (TS10) or two TSs (TS5 and TS4). From MIN4, as expected on the basis of the general mechanism, the reaction also proceeds to form PN via either a one- or two-step process. A full account of the energetics is provided in Table 1, which reports—for each relevant stationary point—the junChS, revDSD/junTZ, and CASPT2/augTZ relative energies with and without inclusion of the ZPE correction.

The accuracy of the junChS scheme for energy evaluations of reactive systems has been demonstrated in Alessandrini et al. (2021), Barone et al. (2021), and Ye et al. (2023), but the

present work also offers an additional comparison of such energies with those resulting from CASPT2/augTZ calculations. These allow us to inspect the potential multi-reference character of the stationary points to be considered in the subsequent kinetic study. From the inspection of Table 1, a similar energy trend is observed for the junChS, CASPT2, and revDSD relative energies, with the junChS model providing the largest energy values and CASPT2 lying in between junChS and revDSD. The largest differences are observed for TS6 and TS7, for which CASPT2 provides relative energies that are more than halved with respect to those obtained with the other two methodologies. This might be related to a multi-reference character of these two TSs or to the active space employed, which cannot uniformly describe all the intermediates of the reaction. However, we note that in all cases the TSs are still submerged with respect to the reactants, and that they tend to further disfavor the pathway toward the PN product.

In view of the differences noticed in the entrance channels for  $CH_2NH + C_3N$  with respect to the general mechanism and the lack of a kinetic study for  $CH_2NH + CP$ , this reaction has been re-investigated, the resulting PES being depicted in Figure 4 (the relative energies of each stationary point are instead reported in Table 4 in Appendix C). The re-investigation has also been prompted by the different levels of theory employed by Alessandrini et al. (2021) for the reactive PES characterization. The inspection of Figure 4 confirms the general mechanism and the reaction paths derived by Alessandrini et al. (2021). However, differences emerged in the entrance channel. Indeed, a weak pre-reactive complex (MIN6) has been located. This leads to MIN4 and MIN1z via TS9 and TS10, respectively. Since TS10 lies above the reactants, the only open path in the ISM is through MIN4, which can still evolve to MIN1z via the formation of MIN3. Overall, the formation path of PN is the same as that predicted by the general mechanism, while PZ and PE can be produced only through a longer pathway involving at least three TSs for the former and four TSs for the latter. Since some exothermic H-abstraction processes were found for the other radicals, these have been investigated also for CP. The corresponding energies are summarized in Table 4. The most relevant H-abstraction

**Table 1**  
Relative Energies (Kilojoule per Mole) of the Stationary Points of the CH<sub>2</sub>NH + C<sub>3</sub>N Reaction

	revDSD/junTZ		junChS		CASPT2/aug-cc-pVTZ	
	Energy	ZPE Corrected <sup>a</sup>	Energy	ZPE Corrected <sup>a</sup>	Energy	ZPE Corrected <sup>a</sup>
MIN1e	-280.85	-278.22	-256.88	-254.26	-251.47	-248.85
MIN1z	-282.52	-280.11	-258.34	-255.93	-252.77	-250.36
MIN2	-366.85	-355.94	-361.24	-350.32	-358.35	-347.43
MIN3	-229.29	-218.93	-224.33	-213.97	-210.95	-200.59
MIN4	-294.99	-291.77	-274.16	-270.95	-271.19	-267.97
MIN5	-320.89	-315.62	-316.94	-311.67	-305.02	-299.75
MIN6	-99.37	-90.14	-84.98	-75.75	-92.99	-83.76
MIN7	-118.95	-107.93	-98.62	-87.60	-117.50	-106.48
MIN8	-261.53	-253.44	-257.81	-249.71	-258.80	-250.71
MIN9	-128.51	-119.92	-129.80	-121.21	...	...
MIN10	-134.99	-126.76	-135.81	-127.58	...	...
MIN11	-64.98	-68.83	-71.26	-75.11	...	...
TSi	-272.16	-270.22	-247.87	-245.94	-242.69	-240.76
TS1e	-103.57	-115.91	-96.44	-108.78	-93.32	-105.66
TS1z	-105.50	-117.34	-98.86	-110.70	-95.64	-107.48
TS2e	-130.76	-132.30	-121.16	-122.70	-129.64	-131.18
TS2z	-136.86	-137.98	-127.12	-128.24	-135.53	-136.65
TS3e	-115.22	-125.28	-107.94	-118.00	-101.54	-111.60
TS3z	-115.93	-125.76	-109.53	-119.36	-102.85	-112.68
TS4	-185.26	-178.70	-186.32	-179.76	-173.49	-169.81
TS5	-175.76	-172.09	-172.52	-168.84	-185.76	-179.20
TS6	-78.62	-91.89	-66.37	-79.65	-20.13	-33.40
TS7	-104.24	-108.89	-91.95	-96.60	-40.87	-45.52
TS8	-94.25	-107.28	-87.75	-100.78	-82.06	-95.08
TS9	-19.52	-19.12	-17.88	-17.48	-11.06	-10.66
TS10	-36.74	-38.57	-26.19	-28.02	-23.10	-24.84
TS11	-77.71	-72.71	-63.92	-58.92	-71.57	-66.58
TS12	-36.85	-41.22	-25.88	-30.25	-41.45	-45.82
TS13	-127.59	-131.00	-141.56	-144.96	-141.07	-144.47
TS14	12.03	7.16	8.43	3.57	...	...
TS15	43.46	41.50	32.22	30.25	...	...
TS16	-78.74	-79.54	-93.41	-94.21	...	...
TS17	-63.43	-64.57	-67.10	-68.23	...	...
TS18	69.85	53.29	40.96	24.40	...	...
TS19	-29.52	-39.33	-66.75	-66.94	...	...
PE	-142.86	-165.04	-120.12	-142.30	-130.17	-152.34
PZ	-144.94	-166.74	-122.09	-143.90	-131.90	-153.71
PN	-118.61	-142.31	-94.14	-117.84	-102.49	-126.18
PH1	-217.81	-231.57	-206.83	-220.59	-203.84	-217.60
PH2	-169.68	-185.42	-155.24	-170.99	...	...
PH3	-191.30	-204.65	-175.96	-189.31	...	...

**Notes.**

<sup>a</sup> Harmonic ZPE corrections calculated at the revDSD/junTZ level of theory.

path is that leading to PH2 (HCP + *cis*-HCNH, see Figure 4). This lies by about 91 kJ mol<sup>-1</sup> below the reactants, but it is formed via a TS (TS11), which emerges by about 8 kJ mol<sup>-1</sup> (at the junChS level of theory including ZPE). Even if this reaction might occur via H-atom tunneling, we did not include it in our kinetic estimates reported in the following. Other possible H-abstraction paths, also reported in Figure 4, are those leading to PH1 and PH3. It is noted that they are similar to those for the C<sub>3</sub>N + CH<sub>2</sub>NH reaction and involve high emerged barriers. For example, PH1 is formed in two steps from MIN1z in analogy to the emerged path discussed in the case of C<sub>3</sub>N. Since all H-abstraction pathways involve one or more TSs lying above the reactants, their contribution to kinetics is not relevant in the present study and thus not considered.

From the comparison of Figures 3 and 4, it is noted that the entrance channels of the CH<sub>2</sub>NH + C<sub>3</sub>N and CH<sub>2</sub>NH + CP reactions are slightly different. In addition to what was noted above, a clear difference is that the C<sub>3</sub>N radical reacting with CH<sub>2</sub>NH forms the MIN6 intermediate that evolves (through submerged barriers) into MIN4 and MIN1z, while—in the case of the CP radical—MIN6 is a pre-reactive complex and the barrier connecting it to MIN1z is emerged (by about 6 kJ mol<sup>-1</sup>; that to MIN4 is instead still submerged). Furthermore, on the CH<sub>2</sub>NH + C<sub>3</sub>N PES, MIN4 can be also accessed directly, while this is not the case for CH<sub>2</sub>NH + CP. The accurate and detailed investigation of these two reactive PESs suggests that the general mechanism holds, but differences can emerge in the entrance channels. Particular attention should thus be given to understanding whether pre-reactive complexes (and the corresponding



**Table 2**  
Arrhenius–Kooij Parameters for the CH<sub>2</sub>NH + CP and CH<sub>2</sub>NH + C<sub>3</sub>N Reactions<sup>a</sup>

CH <sub>2</sub> NH + CP				
Fit parameter	PE	PZ	PN	...
$\alpha/\text{cm}^{-3} \text{ molecule}^{-1} \text{ s}^{-1}$	$4.31 \times 10^{-12}$	$1.50 \times 10^{-11}$	$1.14 \times 10^{-12}$	...
$\beta$	0.37	0.23	0.52	...
$\gamma/\text{K}$	-86.91	-79.05	-94.95	...
rms <sup>b</sup>	$5.26 \times 10^{-13}$	$1.81 \times 10^{-12}$	$1.41 \times 10^{-13}$	...
CH <sub>2</sub> NH + C <sub>3</sub> N				
Fit parameter	PE	PZ	PN	PH1
$\alpha/\text{cm}^{-3} \text{ molecule}^{-1} \text{ s}^{-1}$	$4.05 \times 10^{-10}$	$5.00 \times 10^{-10}$	$3.13 \times 10^{-11}$	$1.58 \times 10^{-11}$
$\beta$	-0.13	-0.13	0.15	-0.93
$\gamma/\text{K}$	24.33	24.31	3.99	76.33
rms <sup>b</sup>	$2.70 \times 10^{-12}$	$3.74 \times 10^{-12}$	$5.64 \times 10^{-14}$	$4.25 \times 10^{-13}$

**Notes.**

<sup>a</sup> Fit of the rate constants obtained using the junChS energies corrected for harmonic ZPE contributions at the revDSD/junTZ level.

<sup>b</sup> rms stands for root-mean-square deviation of the fit.

temperature, the pre-reactive complex of the CH<sub>2</sub>NH + CP reaction only evolves toward MIN4, the kinetic outcomes are in line with the thermodynamic results: the reaction follows the lowest energy pathway, forming first MIN1z and then PZ and PE, while the path toward PN is less favored because of higher barriers to be overcome.

For the CH<sub>2</sub>NH + C<sub>3</sub>N reaction, the global rate constants for the PE (black squares), PZ (red bullets), PN (cyan triangles), and PH1 (green reversed triangles) products are shown in Figure 6. Panel (a) reports the pressure dependence at 100 K, while the insets (b)–(e) show how the rate coefficients of each product vary with temperature in the low-pressure limit regime ( $1 \times 10^{-12}$  atm). The formation of PH1 (HC<sub>3</sub>N + CH<sub>2</sub>N) is independent of pressure, as can be seen in panel (a), and its rate constant shows a non-Arrhenius behavior from 300 K down to 80 K, while below such temperature decreases with temperature (see panel (e) of Figure 6). It is also noted that the channel leading to PH1 is the slowest one, with a rate coefficient of about  $2.0 \times 10^{-11} \text{ cm}^3 \text{ molecule}^{-1} \text{ s}^{-1}$ . This is followed by the formation of PN. For this latter, the rate coefficient shows some dependence on pressure, but the low-pressure regime is already reached at  $1 \times 10^{-4}$  atm (see panel (a)). For this channel, a typical Arrhenius behavior is noted (panel (d)), with a rate constant— at 40 K—of  $2.1 \times 10^{-11} \text{ cm}^3 \text{ molecule}^{-1} \text{ s}^{-1}$ , thus in competition with the formation of PH1. The formation of both PE and PZ is one order of magnitude faster, and they show very similar behaviors for both pressure and temperature dependence of the rate coefficients. From panel (a), it is evident that already at  $1 \times 10^{-3}$  atm the low-pressure limit is nearly obtained. Concerning the temperature dependence, panels (b) and (c) of Figure 6 show a mixed behavior: the non-Arrhenius one is followed down from 300 K to  $\sim 180$  K, while below that temperature the rate coefficient strongly decreases with temperature. At 40 K, the formation of PE and PZ proceeds at a rate of about  $3\text{--}2 \times 10^{-11}$  and  $3.9 \times 10^{-11} \text{ cm}^3 \text{ molecule}^{-1} \text{ s}^{-1}$ , respectively.

As already mentioned, the temperature dependence of rate constants has been modeled using the Arrhenius–Kooij equation, whose expression can be found in Appendix A (Equation (A5)) and the corresponding results in Table 2. These parameters can be used to extrapolate the rate coefficients at temperatures below 40 K and suggest that, for

both reactions, all products can be formed in the ISM conditions, with the PZ product being the most favored. However, at very low temperatures also the quantum tunneling of H atoms could be effective, thus opening the pathway to the formation of PH2 (and PH3 to a lesser extent) for both the CH<sub>2</sub>NH + C<sub>3</sub>N and CH<sub>2</sub>NH + CP reactions and PH1 for the latter process.

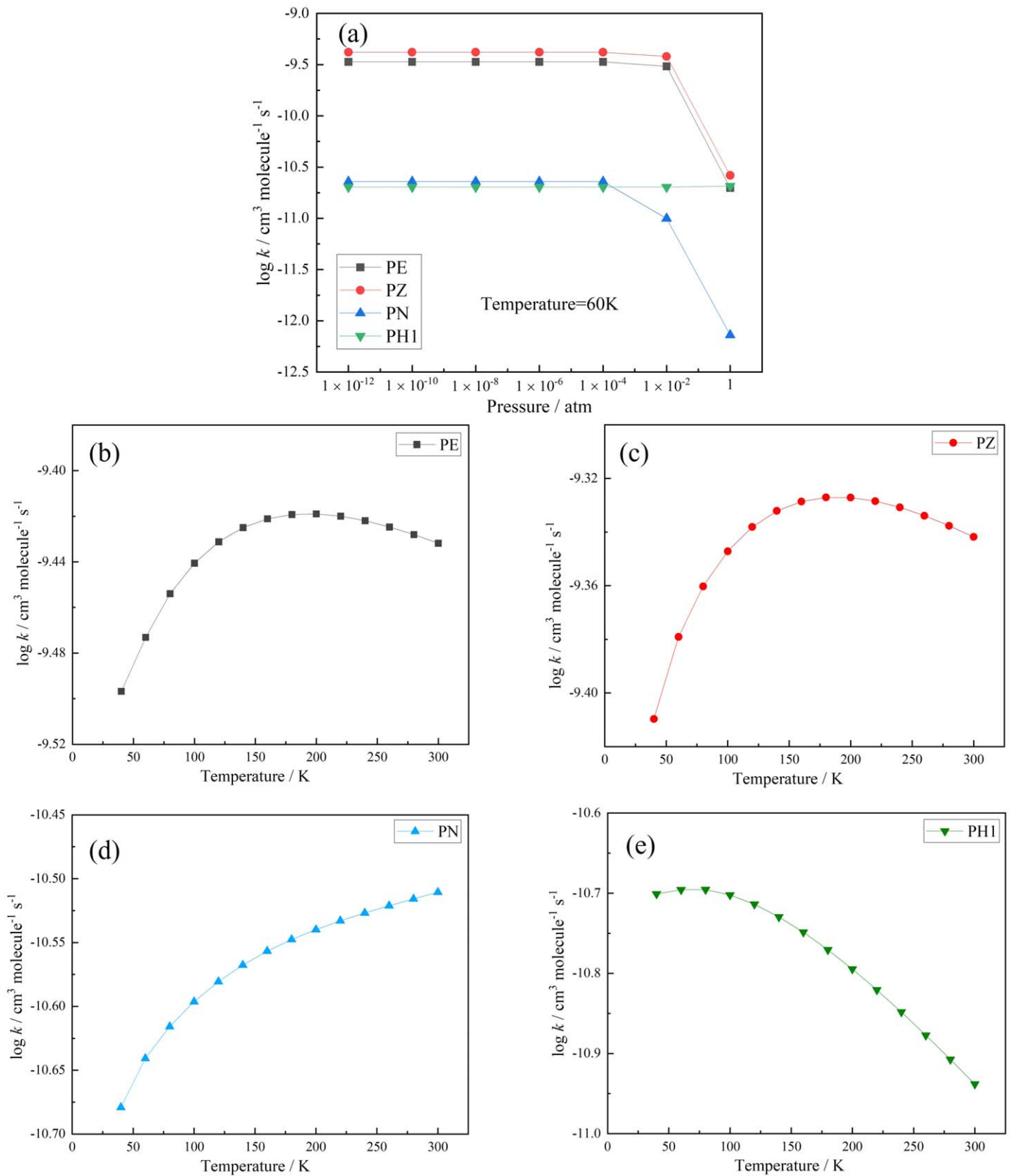
### 3.3.1. Spectroscopic Characterization

Based on the results collected in Figure 3 and Table 1, the CH<sub>2</sub>CN + C<sub>3</sub>N reaction can take place at the low temperatures of the ISM. As a consequence, novel complex imines are suggested as new potential candidates for astronomical observations. However, to the best of our knowledge, no spectroscopic characterization is available for them, which is instead required to guide astronomical searches. As a first step toward the rotational spectroscopy investigation in the laboratory (which will provide the line catalog), in this work, we report the first accurate structural characterization and the corresponding rotational constants for CH<sub>2</sub>NC<sub>3</sub>N (PN) and both *Z*- and *E*-HNCHC<sub>3</sub>N isomers (PZ and PE). While a graphical overview of these molecules is provided in Figure 7, the structural parameters and rotational constants are collected in Table 3. As mentioned in the computational details section, the TM+LR approach has been employed to obtain an accurate structural characterization. As demonstrated in Ye et al. (2022), TM+LR equilibrium rotational constants augmented by B3LYP/junDZ vibrational corrections are able to reproduce experimental ground-state rotational constants with a relative accuracy of about 0.02%–0.05%. For the structural and spectroscopic characterization of the products of the CH<sub>2</sub>NH + CP reaction, the reader is referred to Alessandrini et al. (2021).

## 4. Conclusions

The present work investigated the validity and applicability of the general mechanism proposed in Puzzarini (2022) for the gas-phase reaction between methanimine and a small radical. Seven radicals, already detected in the ISM, have been considered as partners in the reaction with methanimine; these range from diatomics (NO, NS, SH, and SiN) to triatomics

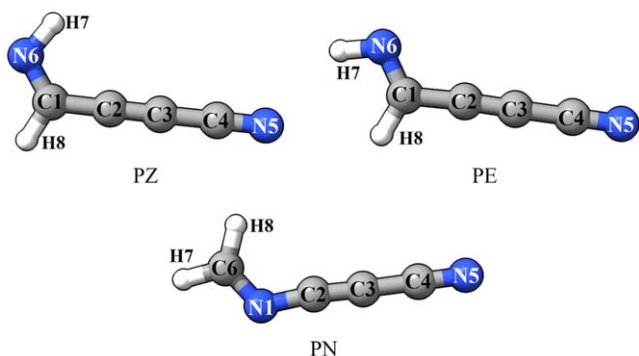




**Figure 6.** The  $\text{CH}_2\text{NH} + \text{C}_3\text{N}$  reaction kinetics. Panel (a) shows the pressure dependence of the rate constants at  $T = 100 \text{ K}$ ; panels (b)–(e) report the temperature dependence at  $p = 1 \times 10^{-12} \text{ atm}$  for the PE, PZ, PN, and PH1 products, respectively.

(HCO and HCS) and one linear tetratomic species ( $\text{C}_3\text{N}$ ). The preliminary thermochemical study pointed out that the only reaction between  $\text{CH}_2\text{NH}$  and  $\text{C}_3\text{N}$  is exothermic and thus of potential interest to interstellar chemistry. The first finding is

that any general mechanism requires a preliminary screening to discriminate between endothermic reactions that need to be discarded and exothermic processes that deserve further investigation.



**Figure 7.** Molecular structures and atom labeling of *Z*-HNCHC<sub>3</sub>N (PZ), *E*-HNCHC<sub>3</sub>N (PE), and CH<sub>2</sub>NC<sub>3</sub>N (PN).

**Table 3**

Structural Parameters,<sup>a</sup> Equilibrium Rotational Constants, and Corresponding Vibrational Corrections<sup>b</sup> for *Z*-HNCHC<sub>3</sub>N (PZ), *E*-HNCHC<sub>3</sub>N (PE), and CH<sub>2</sub>NC<sub>3</sub>N (PN)

Parameter	PZ	PE	PN
$r(\text{H7N6})/r(\text{H8C6})$	1.020	1.019	1.087
$r(\text{C1N6})/r(\text{H7C6})$	1.277	1.276	1.082
$r(\text{C1H8})/r(\text{N1C6})$	1.086	1.090	1.279
$r(\text{C1C2})/r(\text{N1C2})$	1.436	1.435	1.333
$r(\text{C2C3})$	1.211	1.210	1.213
$r(\text{C3C4})$	1.374	1.374	1.370
$r(\text{C4N5})$	1.161	1.161	1.162
$\angle(\text{H7N6C1})/\angle(\text{H7C6H8})$	110.60	109.74	118.96
$\angle(\text{N6C1H8})/\angle(\text{N1C6H8})$	118.63	124.44	123.18
$\angle(\text{C2C1N6})/\angle(\text{C2N1C6})$	125.11	120.38	120.35
$\angle(\text{C3C2C1})/\angle(\text{C3C2N1})$	179.84	177.04	173.43
$\angle(\text{C4C3C2})$	179.69	179.22	178.35
$\angle(\text{N5C4C3})$	179.99	179.71	179.90
$A_e$	42917.434	50359.462	53410.123
$B_e$	1373.804	1358.116	1423.560
$C_e$	1331.192	1322.451	1386.602
$\Delta A_{\text{vib}}$	-806.154	-462.539	-930.452
$\Delta B_{\text{vib}}$	3.810	1.645	3.297
$\Delta C_{\text{vib}}$	3.880	2.192	3.652

#### Notes.

<sup>a</sup> TM+LR structural parameters: bond distances are in angstroms and angles in degrees. See Appendix A for details. For atom labeling, see Figure 7.

<sup>b</sup> TM+LR equilibrium rotational constants and B3LYP/junDZ vibrational corrections. Values are in megahertz.

In view of its possible relevance, the reactive PES of the CH<sub>2</sub>NH + C<sub>3</sub>N reaction has been accurately characterized in order to understand whether it can occur or not in the ISM. Such an analysis pointed out that the reaction proceeds following the general mechanism proposed in the literature (Pazzarini 2022), thus further demonstrating its validity for the formation of complex imines in the ISM. Indeed, in addition to being exothermic, the CH<sub>2</sub>NH + C<sub>3</sub>N reaction presents barrierless entrance channels and only submerged barriers. As a result, this reaction suggests new molecules to be searched for in space, namely, *Z*-HCNCHCCCN, *E*-HCNCHCCCN, and CH<sub>2</sub>NCCCN. The H-abstraction process, which forms HC<sub>3</sub>N and CH<sub>2</sub>N, has also been found accessible. To confirm the feasibility of such a reaction in interstellar conditions, kinetic calculations have been performed, providing the global rate

coefficients for each product. Kinetics reveals that all pathways toward the products are feasible even at temperatures as low as 10 K. Together with the CH<sub>2</sub>NH + C<sub>3</sub>N reaction, that between CH<sub>2</sub>NH and the CP radical has been re-examined, thus showing—differently from the previous study—the presence of a pre-reactive complex that governs the entrance channel. The comparison of the two reactive PESs in the region where the reactants approach, points out some differences. Indeed, the second finding of this study is that, while the general mechanism is valid and confirmed for the evolution of the system from the first stable intermediates toward the products, the reactants approach region needs to be carefully investigated because it seems to be highly system dependent. Further work is here needed to understand whether a rationalization can be derived as well. For these two reactions, the H-abstraction mechanisms have also been studied in detail. Our work seems to suggest that similar mechanisms apply to those paths that start from stable minima of the PES. Instead, H-abstractions that involve pre-reactive complexes or reactants have to be specifically derived for the reaction under consideration. Moving to kinetic simulations, the two reactions show different behaviors as a result of the differences in the PES features, and mainly in barrier heights. While non-Arrhenius temperature dependence is noted for all CH<sub>2</sub>NH + CP pathways, a mixed trend is observed for the CH<sub>2</sub>NH + C<sub>3</sub>N processes. However, in all cases, the magnitude of the rate constants at very low temperatures is such that the formation of all products is competitive in the ISM.

The PE, PZ, and PN products of the CH<sub>2</sub>NH + C<sub>3</sub>N reaction belong to the C<sub>4</sub>H<sub>2</sub>N<sub>2</sub> family of compounds, which is of astrochemical relevance (Marchione et al. 2022), but they have not previously been studied. Investigations on the entire isomeric family are currently in progress by exploiting a protocol recently implemented (Alessandrini et al. 2023). To enable the first experimental characterization of *Z*-HCNCHCCCN, *E*-HCNCHCCCN, and CH<sub>2</sub>NCCCN by means of rotational spectroscopy, we have also reported accurate predictions for their rotational constants.

Finally, the possibility of having quantum tunneling of H atoms in processes that involve TSs lying above the reactants has been discussed for the reaction involving methanimine with the HCS, SH, and CP radicals.

#### Acknowledgments

This work has been supported by MUR (PRIN grant No. 202082CE3T) and by the University of Bologna (RFO funds). H.Y. thanks the China Scholarship Council (CSC) for financial support. The COST Action CA21101 “COSY—Confined molecular systems: from a new generation of materials to the stars” is acknowledged.

#### Appendix A Computational Details

In the following three sections, a thorough account of the computational details with respect to those provided in the main text is reported. All Density Functional Theory computations and single-point energy calculations within the junChS model have been performed with the Gaussian 16 suite of programs (Frisch et al. 2016), while for CASPT2 computations, the MOLPRO program package (Werner et al. 2023) has been employed.

### A.1. Thermochemistry

As mentioned in the main text, the junChS model was employed to derive the accurate thermochemistry reported in the present work. This scheme starts from the energy evaluation using the coupled-cluster (CC) singles, doubles, and perturbative triples method (CCSD(T); Raghavachari et al. 1989) in conjunction with the jun-cc-pVTZ basis set, within the frozen-core (fc) approximation. Then, two corrections are added in order to account for the extrapolation to the complete basis set (CBS) limit and core-valence (CV) correlation effects. These terms are computed using Møller–Plesset perturbation theory to the second order (MP2; Møller & Plesset 1934) and incorporated in the scheme as follows:

$$E(\text{junChS}) = E(\text{CCSD(T)}/\text{jun-cc-pVTZ}) + \Delta E_{\text{MP2}}^{\text{CBS}} + \Delta E_{\text{MP2}}^{\text{CV}}. \quad (\text{A1})$$

The  $\Delta E_{\text{MP2}}^{\text{CBS}}$  term recovers the error due to the basis set truncation (within the fc approximation), while the second correction ( $\Delta E_{\text{MP2}}^{\text{CV}}$ ) accounts for the effects of correlating inner electrons. The CBS term is evaluated by exploiting the  $n^{-3}$  extrapolation formula (Helgaker et al. 1997) in combination with the jun-cc-pVTZ ( $n = 3$ ) and jun-cc-pVQZ ( $n = 4$ ) basis sets, as follows:

$$\Delta E_{\text{MP2}}^{\text{CBS}} = \frac{4^3 E_{\text{fc-MP2}}^{\text{jun-cc-pVQZ}} - 3^3 E_{\text{fc-MP2}}^{\text{jun-cc-pVTZ}}}{4^3 - 3^3} - E_{\text{fc-MP2}}^{\text{jun-cc-pVTZ}}. \quad (\text{A2})$$

The CV term is calculated as the difference between two energy computations:

$$\Delta E_{\text{MP2}}^{\text{CV}} = E_{\text{ae-MP2/cc-pwCVTZ}} - E_{\text{fc-MP2/cc-pwCVTZ}}, \quad (\text{A3})$$

where the first term on the right-hand side is the energy evaluated with all electrons correlated (ae), while the second one provides the energy within the fc approximation. Both calculations employ the cc-pwCVTZ basis set (Peterson & Dunning 2002).

Since open-shell species might be affected by spin-contamination, the spin-restricted open-shell Hartree–Fock wave function (Gauss et al. 1991; Lauderdale et al. 1991, 1992; Watts et al. 1993; Puzzarini & Barone 2020) is used as a reference in all calculations of the junChS model. This methodology was already employed in Alessandrini et al. (2021) and led to energies that agree, within  $1 \text{ kJ mol}^{-1}$ , with those computed using the so-called HEAT-like approach (Tajti et al. 2004; Bomble et al. 2006; Harding et al. 2008; Puzzarini & Barone 2020; Puzzarini et al. 2020), which is known to provide sub-kJ mol<sup>-1</sup> accuracy. This good performance of junChS has also been recently demonstrated in Ye et al. (2023).

### A.2. Kinetics

As explained in the main manuscript, the junChS energies were employed in kinetic calculations based on AITSTME. The barrierless approach between the two reactants has been modeled using PST, with the rate constant being determined by

an  $r^{-6}$  attractive potential:

$$V_{\text{eff}} = V(R_0) - \frac{C_6}{r^6}, \quad (\text{A4})$$

where  $V(R_0)$  is the energy of the two separated reactants and  $r$  the long-range distance between the two fragments. The latter was chosen as the C–C distance in the case of  $\text{CH}_2\text{NH} + \text{CP}$ . For the reaction between methanimine and  $\text{C}_3\text{N}$ , the distance between the C-end of the radical and the N-atom of methanimine was chosen for the entrance channel toward MIN4, while the distance between the N-atom of  $\text{CH}_2\text{NH}$  and the central carbon of the  $\text{C}_3\text{N}$  radical was considered for the entrance channel toward MIN6. The potentials were obtained from rigid scans of  $r$  from 2.5–10 Å, with the potential energies being fitted to derive the  $C_6$  parameter of Equation (A4).

After the entrance channel, all the other steps have been modeled using conventional TST (Fernández-Ramos et al. 2006) and employing the rigid-rotor harmonic-oscillator approximation. Tunneling effects have also been taken into account by means of the Eckart model (Eckart 1930).

To model the temperature dependence of the global rate coefficients the Arrhenius–Kooij expression (Kooij 1893) has been employed:

$$k(T) = \alpha \left( \frac{T}{300} \right)^\beta \exp \left( -\frac{\gamma}{T} \right), \quad (\text{A5})$$

where  $\alpha$ ,  $\beta$ , and  $\gamma$  are the fitting parameters.

### A.3. Spectroscopic Characterization

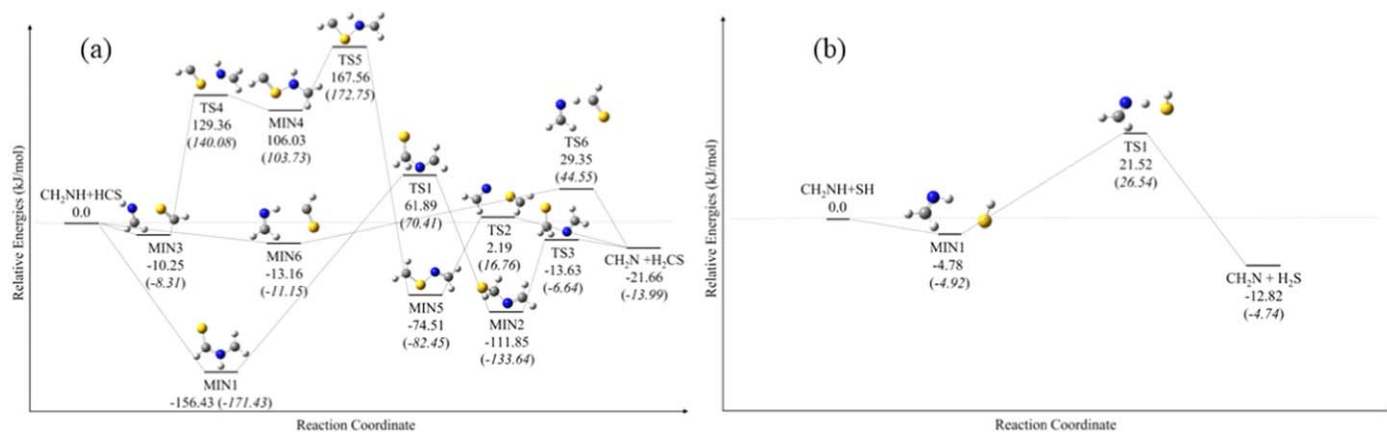
As mentioned in the main text, the TM+LR approach has been employed to derive accurate equilibrium structures for the PE, PZ, and PN products of the  $\text{CH}_2\text{NH} + \text{C}_3\text{N}$  reaction. As explained in Melli et al. (2021), TM+LR uses the TM approach (Piccardo et al. 2015), which allows for improving the geometry of a molecule starting from the accurate structure of its fragments:

$$r_e^T(\text{TM}) = r_e^T(\text{revDSD}) + \Delta r_e^F(\text{TM}), \quad (\text{A6})$$

where  $r$  denotes a generic structural parameter. Here,  $r_e^T(\text{TM})$  is the TM-corrected structure of the target molecule, while  $r_e^T(\text{revDSD})$  is the structure of the target molecule at the revDSD/junTZ level and  $\Delta r_e^F(\text{TM})$  is the correction provided by the TM approach. The latter is computed as follows:

$$\Delta r_e^F(\text{TM}) = r_{\text{acc}}^F - r_e^F(\text{revDSD}), \quad (\text{A7})$$

where  $r_{\text{acc}}^F$  is the accurate structure of the fragment and  $r_e^F(\text{revDSD})$  its revDSD/junTZ counterpart. In the present case,  $\text{CH}_2\text{NH}$  and  $\text{HC}_3\text{N}$  have been envisaged as TM fragments for both  $\text{HNCHC}_3\text{N}$  and  $\text{CH}_2\text{NHC}_3\text{N}$ . For both  $\text{CH}_2\text{NH}$  and  $\text{HC}_3\text{N}$ , the  $r_{\text{acc}}$  values used are those of the so-called semi-experimental equilibrium structure, which is already available in the literature (see Botschwina et al. 1993 for  $\text{HC}_3\text{N}$  and Mendolicchio et al. 2017 for  $\text{CH}_2\text{NH}$ ). While the TM approach allows for correcting the geometrical parameters of the fragments forming the target molecule, one also needs to adjust the linkage parameters, i.e., those connecting the two



**Figure 8.** H-abstraction mechanisms for the CH<sub>2</sub>NH + HCS (panel (a)) and CH<sub>2</sub>NH + SH (panel (b)) reactions. The junChS relative energies corrected for the harmonic revDSD/junTZ ZPE contribution are reported (in parentheses, the energetics at the revDSD/junTZ level of theory corrected for the corresponding harmonic ZPE is given).

fragments. If these are kept fixed at the revDSD/junTZ level, one then resorts to the TM model. If the linkage distances are corrected using the LR parameters reported in Ceselin et al. (2021), one then resorts to the TM+LR model. The reader is referred to Ye et al. (2022) for a thorough account of the improvement obtained once moving from TM to TM+LR.

From the equilibrium structure, the equilibrium rotational constants are straightforwardly derived (Puzzarini et al. 2008, 2010). Despite the fact that equilibrium rotational constants account for 99% (or more) of the vibrational ground-state rotational constants (Puzzarini & Stanton 2023), which are those of interest for rotational spectra prediction, vibrational corrections need to be incorporated when aiming at high accuracy. Within the second-order vibrational perturbation theory (Mills 1972; Barone 2005), vibrational ground-state rotational constants ( $B_0^i$ ) can be written as the combination of equilibrium rotational constants ( $B_e^i$ ) and the corresponding vibrational corrections ( $\Delta B_{\text{vib}}^i$ ):

$$B_0^i = B_e^i + \Delta B_{\text{vib}}^i = B_e^i - \frac{1}{2} \sum_r \alpha_r^i, \quad (\text{A8})$$

where  $i$  refers to the  $i$ th inertial axis ( $i = a, b, \text{ and } c$ , so—for example— $B^a$  is denoted as  $A$ ). In the equation above,  $\alpha_r^i$  is the vibration-rotation interaction constant, with  $r$  denoting the  $r$ th vibrational normal mode. The  $\alpha_r^i$  values are obtained through anharmonic force field computations, which have been carried out at the B3LYP/junDZ level.

## Appendix B H-abstraction Mechanisms

The energetic study carried out in Section 3.1 indicates that the HCS and SH radicals can extract one H-atom from methanimine to form the corresponding closed-shell species (H<sub>2</sub>CS and H<sub>2</sub>S) and H<sub>2</sub>CN as a coproduct. Since these processes are exothermic (by about 22 and 12 kJ mol<sup>-1</sup>, respectively), the corresponding potential energy surface has been investigated.

Three different paths have been observed for H<sub>2</sub>CS + H<sub>2</sub>CN, which are reported in Figure 8, panel (a): it

is evident that, in all cases, H-abstraction occurs via emerged (with respect to the reactants' energy) transition states. First, the HCS radical can form the bounded MIN1 (−156.4 kJ mol<sup>-1</sup>) intermediate from the addition of the C-atom of the radical to the N-atom of CH<sub>2</sub>NH. Then, MIN1 evolves via a barrier of 217 kJ mol<sup>-1</sup> (TS1 lying 61 kJ mol<sup>-1</sup> above the reactants) to MIN2. The products are then formed via TS3. The second path starts from a pre-reactive complex (MIN3), located at −10 kJ mol<sup>-1</sup> with respect to the reactants, which evolves to MIN4 via TS4 (130 kJ mol<sup>-1</sup>). MIN4 is the addition of the S-atom of the HCS radical to the N-atom of CH<sub>2</sub>NH. This forms MIN5 via TS5 (lying 170 kJ mol<sup>-1</sup> higher in energy than the reactants). MIN5 evolves to HCS + H<sub>2</sub>CN by overcoming TS8, which is still slightly emerged by about 2 kJ mol<sup>-1</sup> at the junChS level. The third path observed on the PES is that originating from a second pre-reactive complex (MIN6) and leading to the products in a single step involving TS9 (29.35 kJ mol<sup>-1</sup>). While this path is not a submerged one, it might occur via quantum tunneling, making this pathway a channel of interest at the low temperatures of the ISM. Since all the other products of the CH<sub>2</sub>NH + HCS reaction investigated in the present work resulted to be endothermic, our calculations suggest that this H-abstraction channel is the main path of the reaction.

For the reaction of the SH radical with methanimine, H-abstraction is somewhat similar to the third path of CH<sub>2</sub>NH + HCS, as shown in Figure 8, panel (b). The reactants form a pre-reactive complex, indicated as MIN1, which then evolves into H<sub>2</sub>S + H<sub>2</sub>CN via TS1 located 21 kJ mol<sup>-1</sup> above the reactants. Thus, H-atom quantum tunneling could also play a role in the CH<sub>2</sub>NH + SH reaction and it is probably the only relevant pathway between the two species.

## Appendix C Additional Data for the CH<sub>2</sub>NH+CP Reaction

In this section, for the CH<sub>2</sub>NH + CP reaction, the revDSD/junTZ and junChS relative energies, with and without inclusion of ZPE contribution, are collected in Table 4.






**Table 4**  
Relative Energies (Kilojoule per Mole) of the Stationary Points of the CH<sub>2</sub>NH + CP Reaction

	revDSD/junTZ		junChS	
	Energy	ZPE Corrected <sup>a</sup>	Energy	ZPE Corrected <sup>a</sup>
MIN1e	-224.34	-213.75	-184.02	-173.43
MIN1z	-228.88	-218.98	-184.02	-174.12
MIN2	-335.42	-323.52	-306.21	-294.31
MIN3	-239.32	-225.92	-200.12	-186.72
MIN4	-259.33	-253.06	-218.52	-212.25
MIN5	-338.26	-326.62	-295.43	-283.78
MIN6	-8.19	-5.98	-7.31	-5.13
MIN7	-134.12	-123.45	-101.42	-90.79
MIN8	-60.00	-54.90	-48.71	-46.40
MIN9	-130.57	-119.51	-98.25	-87.22
TSi	-218.95	-210.34	-173.07	-164.46
TS1e	-76.39	-83.94	-27.59	-39.03
TS1z	-81.66	-87.84	-56.07	-58.36
TS2e	-79.98	-80.03	-53.14	-53.18
TS2z	-88.99	-88.56	-61.72	-61.28
TS3e	-60.63	-69.82	-36.92	-46.11
TS3z	-63.99	-73.36	-41.54	-50.91
TS4	-161.80	-156.17	-132.35	-126.71
TS5	-164.00	-154.79	-140.47	-131.25
TS6	-37.48	-47.05	-2.44	-12.01
TS7	-68.81	-71.91	-37.68	-40.78
TS8	-51.61	-65.14	-28.77	-42.29
TS9	-5.23	-3.89	-4.24	-2.94
TS10	4.73	8.63	2.39	6.25
TS11	9.39	0.73	17.05	8.35
TS12	31.69	29.45	61.42	59.13
TS13	73.08	64.37	78.64	69.89
TS14	-3.41	-5.33	-4.39	-6.30
TS15	26.06	23.91	48.71	36.60
TS16	33.29	30.52	0.87	-1.94
TS17	-45.26	-44.78	-23.68	-23.25
PE	-95.12	-112.86	-49.96	-67.70
PZ	-99.87	-117.14	-54.70	-71.97
PN	-81.76	-101.06	-34.49	-53.78
PH1	-164.15	-173.83	-130.78	-140.50
PH2	-116.01	-127.68	-79.18	-90.89
PH3	-137.63	-146.90	-99.91	-111.61

**Notes.**

<sup>a</sup> Harmonic ZPE correction computed at the revDSD/junTZ level.

**ORCID iDs**

Hexu Ye  <https://orcid.org/0000-0002-6023-8913>  
 Silvia Alessandrini  <https://orcid.org/0000-0003-3152-3261>  
 Cristina Puzzarini  <https://orcid.org/0000-0002-2395-8532>

**References**

- Agúndez, M., Marcelino, N., Cernicharo, J., & Tafalla, M. 2018, *A&A*, **611**, L1
- Alessandrini, S., Barone, V., & Puzzarini, C. 2019, *J. Chem. Theory Comput.*, **16**, 988
- Alessandrini, S., Melosso, M., Rivilla, V. M., Bizzocchi, L., & Puzzarini, C. 2023, *Molecules*, **28**, 3226
- Alessandrini, S., Tonolo, F., & Puzzarini, C. 2021, *JChPh*, **154**, 054306
- Andersson, K., Malmqvist, P.-Å., & Roos, B. O. 1992, *JChPh*, **96**, 1218
- Andersson, K., Malmqvist, P. A., Roos, B. O., Sadlej, A. J., & Wolinski, K. 1990, *JPhCh*, **94**, 5483
- Baiano, C., Lupi, J., Tasinato, N., Puzzarini, C., & Barone, V. 2020, *Molecules*, **25**, 2873
- Bao, J. L., & Truhlar, D. G. 2017, *Chem. Soc. Rev.*, **46**, 7548
- Barone, V. 2005, *JChPh*, **122**, 014108
- Barone, V., Lupi, J., Salta, Z., & Tasinato, N. 2021, *J. Chem. Theory Comput.*, **17**, 4913
- Barone, V., & Puzzarini, C. 2022, *FrASS*, **8**, 814384
- Becke, A. D. 1988, *PhRvA*, **38**, 3098
- Bomble, Y. J., Vázquez, J., Kállay, M., et al. 2006, *JChPh*, **125**, 064108
- Botschwina, P., Horn, M., Seeger, S., & Flügge, J. 1993, *MolPh*, **78**, 191
- Celani, P., & Werner, H.-J. 2000, *JChPh*, **112**, 5546
- Cernicharo, J., Agúndez, M., Cabezas, C., et al. 2022a, *EPJWC*, **265**, 00041
- Cernicharo, J., Fuentetaja, R., Cabezas, C., et al. 2022b, *A&A*, **663**, L5
- Ceselin, G., Barone, V., & Tasinato, N. 2021, *J. Chem. Theory Comput.*, **17**, 7290
- Dickens, J., Irvine, W. M., DeVries, C., & Ohishi, M. 1997, *ApJ*, **479**, 307
- Dore, L., Bizzocchi, L., & Degli Esposti, C. 2012, *A&A*, **544**, A19
- Dunning, T. H., Jr. 1989, *JChPh*, **90**, 1007
- Dunning, T. H., Jr., Peterson, K. A., & Wilson, A. K. 2001, *JChPh*, **114**, 9244
- Eckart, C. 1930, *PhRv*, **35**, 1303
- Fernández-Ramos, A., Miller, J. A., Klippenstein, S. J., & Truhlar, D. G. 2006, *ChRv*, **106**, 4518
- Friberg, P., Hjalmarson, A., Guélin, M., & Irvine, W. 1980, *ApJL*, **241**, L99
- Frisch, M. J., Trucks, G. W., Schlegel, H. B., et al. 2016, Gaussian 16 Revision C.01, <https://gaussian.com/>
- Fuentetaja, R., Agúndez, M., Cabezas, C., et al. 2022, *A&A*, **667**, L4
- Fukui, K. 1981, *Acc. Chem. Res.*, **14**, 363

- Gauss, J., Lauderdale, W. J., Stanton, J. F., Watts, J. D., & Bartlett, R. J. 1991, *CPL*, **182**, 207
- Georgievskii, Y., Miller, J. A., Burke, M. P., & Klippenstein, S. J. 2013, *JPCA*, **117**, 12146
- Godfrey, P., Brown, R., Robinson, B., & Sinclair, M. 1973, *ApL*, **13**, 119
- Goerigk, L., & Grimme, S. 2011, *J. Chem. Theory Comput.*, **7**, 291
- Gottlieb, C., Ball, J. A., Gottlieb, E. W., Lada, C., & Penfield, H. 1975, *ApJL*, **200**, L147
- Grimme, S., Ehrlich, S., & Goerigk, L. 2011, *JCoCh*, **32**, 1456
- Harding, M. E., Vázquez, J., Ruscic, B., et al. 2008, *JChPh*, **128**, 114111
- Helgaker, T., Klopper, W., Koch, H., & Noga, J. 1997, *JChPh*, **106**, 9639
- Kendall, R. A., Dunning, T. H., Jr., & Harrison, R. J. 1992, *JChPh*, **96**, 6796
- Kooij, D. M. 1893, *ZPC*, **12**, 155
- Lauderdale, W. J., Stanton, J. F., Gauss, J., Watts, J. D., & Bartlett, R. J. 1991, *CPL*, **187**, 21
- Lauderdale, W. J., Stanton, J. F., Gauss, J., Watts, J. D., & Bartlett, R. J. 1992, *JChPh*, **97**, 6606
- Lee, C., Yang, W., & Parr, R. G. 1988, *PhRvB*, **37**, 785
- Lee, K. L. K., Loomis, R. A., Burkhardt, A. M., et al. 2021, *ApJL*, **908**, L11
- Liszt, H., & Turner, B. 1978, *ApJL*, **224**, L73
- Lupi, J., Puzzarini, C., & Barone, V. 2020, *ApJL*, **903**, L35
- Marchione, D., Mancini, L., Liang, P., et al. 2022, *JPCA*, **126**, 3569
- McGuire, B. A., Burkhardt, A. M., Loomis, R. A., et al. 2020, *ApJL*, **900**, L10
- Melli, A., Tonolo, F., Barone, V., & Puzzarini, C. 2021, *JPCA*, **125**, 9904
- Mendolicchio, M., Penocchio, E., Licari, D., Tasinato, N., & Barone, V. 2017, *J. Chem. Theory Comput.*, **13**, 3060
- Mills, I. M. 1972, in *Molecular Spectroscopy: Modern Research*, ed. K. N. Rao & C. W. Mathews, Vol. 1 (New York: Academic), 115
- Møller, C., & Plesset, M. S. 1934, *PhRv*, **46**, 618
- Neufeld, D., Falgarone, E., Gerin, M., et al. 2012, *A&A*, **542**, L6
- Ocaña, A. J., Blázquez, S., Potapov, A., et al. 2019, *PCCP*, **21**, 6942
- Papajak, E., & Truhlar, D. G. 2011, *J. Chem. Theory Comput.*, **7**, 10
- Peterson, K. A., & Dunning, T. H., Jr. 2002, *JChPh*, **117**, 10548
- Piccardo, M., Penocchio, E., Puzzarini, C., Biczysko, M., & Barone, V. 2015, *JPCA*, **119**, 2058
- Prestage, R. M., Constantikes, K. T., Hunter, T. R., et al. 2009, *Proc. IEEE*, **97**, 1382
- Puzzarini, C. 2020, *FrASS*, **7**, 19
- Puzzarini, C. 2022, *FrASS*, **8**, 811342
- Puzzarini, C., & Barone, V. 2020, *PCCP*, **22**, 6507
- Puzzarini, C., Heckert, M., & Gauss, J. 2008, *JChPh*, **128**, 194108
- Puzzarini, C., Salta, Z., Tasinato, N., et al. 2020, *MNRAS*, **496**, 4298
- Puzzarini, C., & Stanton, J. F. 2023, *PCCP*, **25**, 1421
- Puzzarini, C., Stanton, J. F., & Gauss, J. 2010, *IRPC*, **29**, 273
- Raghavachari, K., Trucks, G. W., Pople, J. A., & Head-Gordon, M. 1989, *CPL*, **157**, 479
- Recio, P., Alessandrini, S., Vanuzzo, G., et al. 2022, *NatCh*, **14**, 1405
- Rivilla, V., Martín-Pintado, J., Jiménez-Serra, I., et al. 2019, *MNRAS Lett.*, **483**, L114
- Roos, B. O., Linse, P., Siegbahn, P. E., & Blomberg, M. R. 1982, *ChPhy*, **66**, 197
- Santra, G., Sylvesty, N., & Martin, J. M. 2019, *JPCA*, **123**, 5129
- Shannon, R. J., Blitz, M. A., Goddard, A., & Heard, D. E. 2013, *NatCh*, **5**, 745
- Shingledecker, C. N., Molpeceres, G., Rivilla, V. M., Majumdar, L., & Kästner, J. 2020, *ApJ*, **897**, 158
- Sita, M. L., Changala, P. B., Xue, C., et al. 2022, *ApJL*, **938**, L12
- Snyder, L., Hollis, J., & Ulich, B. 1976, *ApJL*, **208**, L91
- Sosa, C., & Bernhard Schlegel, H. 1986, *IJCQ*, **29**, 1001
- Tajti, A., Szalay, P. G., Császár, A. G., et al. 2004, *JChPh*, **121**, 11599
- Tercero, F., López-Pérez, J., Gallego, J., et al. 2021, *A&A*, **645**, A37
- Turner, B. 1992, *ApJL*, **388**, L35
- Turner, B., Terzieva, R., & Herbst, E. 1999, *ApJ*, **518**, 699
- Vazart, F., Calderini, D., Puzzarini, C., Skouteris, D., & Barone, V. 2016, *J. Chem. Theory Comput.*, **12**, 5385
- Vazart, F., Latouche, C., Skouteris, D., Balucani, N., & Barone, V. 2015, *ApJ*, **810**, 111
- Watts, J. D., Gauss, J., & Bartlett, R. J. 1993, *JChPh*, **98**, 8718
- Werner, H.-J., Knowles, P. J., Celani, P., et al., 2023 MOLPRO, v2020.2, a Package of ab initio Programs, <https://www.molpro.net/>
- Woon, D. E., & Dunning, T. H., Jr. 1993, *JChPh*, **98**, 1358
- Wootten, A., & Thompson, A. R. 2009, *Proc. IEEE*, **97**, 1463
- Ye, H., Alessandrini, S., Melosso, M., & Puzzarini, C. 2022, *PCCP*, **24**, 23254
- Ye, H., Alessandrini, S., & Puzzarini, C. 2023, *MNRAS*, **525**, 1158